
Article:
Yang, H., Zheng, H., Zhu, Z.Q. orcid.org/0000-0001-7175-3307 et al. (3 more authors) (2019) Comparative study of partitioned stator memory machines with series and parallel hybrid PM configurations. IEEE Transactions on Magnetics, 55 (7). 8106708. ISSN 0018-9464

https://doi.org/10.1109/tmag.2019.2894833

Comparative Study of Partitioned Stator Memory Machines With Series and Parallel Hybrid PM Configurations

Hui Yang[1], Hao Zheng[1], Z. Q. Zhu[2], *Fellow, IEEE*, Heyun Lin[1], Shukang Lyu[1], and Zhenbao Pan[1]

[1]School of Electrical Engineering, Southeast University, Nanjing 210096, China
[2]Department of Electronic and Electrical Engineering, University of Sheffield, Sheffield S1 3JD, U.K.

In this paper, the partitioned stator (PS) structure is extended to variable-flux memory machines, forming two newly emerged PS switched-flux memory machines (PS-SFMMs) with series and parallel hybrid magnet configurations. From the perspective of geometry, both two PS-SFMMs share identical outer stator and rotor segments, while two different types of permanent magnet (PM) arrangements are employed in the inner stationary part. Thus, the developed machines can inherent the geometric separation of the armature winding and PM excitations from the PS design, thus achieving acceptable torque capability, and excellent air-gap flux control. A comparative study between PS-SFMMs with series and parallel structures is established. First, the topologies and operating principle are introduced, respectively. In addition, the design tradeoffs and PM sizing of the two PS machines are revealed and optimized with a simplified magnetic circuit model. Then, the electromagnetic characteristics of PS-SFMMs with different magnetic circuits are investigated and compared with the finite-element (FE) method. The FE results are validated by the experiments on a parallel prototype.

***Index Terms*— Hybrid permanent magnet (PM), memory machine (MM), parallel magnetic circuit, partitioned stator (PS), series magnetic circuit.**

I. Introduction

DUE to the advantages of high torque density and high efficiency, permanent magnet (PM) machines are widely considered as a competitive candidate for electric vehicle applications [1]. Nevertheless, the non-adjustable air-gap flux of the conventional rare-earth PM machines inevitably results in limited constant-power speed range (CPSR). Meanwhile, the required d-axis flux-weakening (FW) current and the associated high copper loss reduces the efficiency particularly at high speeds [2]. Thus, the conventional PM machines generally suffer from a conflict between low-speed high torque and high-speed high power. As a consequence, it is highly desirable to achieve flexible air-gap flux control so as to satisfy the specific requirement over a wide range of loads and speeds [3].

As a viable solution to perform PM magnetization state (MS), the concept of "memory machine (MM)" is proposed and extensively investigated [4]–[17]. Due to the utilization of low coercive force (LCF) PMs, the flexible air-gap flux adjustment can be achieved by applying a temporary current pulse to magnetize LCF PMs. Thus, MSs of LCF PMs can be "memorized" by the corresponding current pulse level. Meanwhile, the associated excitation copper loss is negligible, allowing high-speed loss to be substantially reduced. As a consequence, high efficiency can be maintained within a wide operating range of speeds and loads. In addition, since back electromotive force (EMF) of MM can be controlled due to the variable-flux property so that CPSR can be further extended within the inverter voltage constraint [3]. Due to the above merits, MM is widely recognized as a suitable choice for wide-speed-range applications [5]–[7].

Manuscript received November 6, 2018; accepted January 14, 2019. Corresponding author: H. Yang (e-mail: huiyang@seu.edu.cn).
Digital Object Identifier 10.1109/TMAG.2019.2894833

Generally, MMs can be categorized into ac- and dc-magnetized types according to the winding types supplying the current pulse. Compared to ac-magnetized MMs [4]–[8] resorting to a d-axis current pulse and relatively complicated flux control, dc-magnetized MMs [9]–[17] with auxiliary dc magnetizing coils benefit from more expedient online MS control. The structures of doubly salient [9]–[12] and switched flux [13]–[17] are extended to dc-magnetized MMs. Several advantages such as excellent rotor robustness and easy thermal dissipation can be obtained. Besides, two sets of magnets are used in order to improve the torque density, i.e., NdFeB and LCF PMs. Nevertheless, due to the crowded stator issue in single-stator dc-magnetized MMs [9]–[17], the torque density is inevitably compromised. In order to alleviate this issue, a partitioned stator switched-flux MM (PS-SFMM) is developed [15]–[17]. The armature windings and PMs are separately located on two stators, respectively. The conflict between magnetic and electric loadings is alleviated. Hence, high torque density and energy-efficient flux control capability can be simultaneously realized. However, the previous studies mainly focus on the new topology development [15], [16] and performance analysis [17] in individual cases. Nonetheless, the feasibility of possible magnetic circuits and the corresponding characteristic investigation for the PS-SFMMs remains unreported.

Therefore, to fill this knowledge gap, this paper presents a comparative study of PS-SFMMs with series and parallel hybrid PM configurations. This paper is organized as follows. In Section II, the topologies and operating principle are described, respectively. In Section III, the design tradeoffs and PM sizing of the two PS machines are analytically revealed and optimized with a simplified magnetic circuit model. Then, the electromagnetic characteristics of PS-SFMMs with different magnetic circuits are investigated and compared with

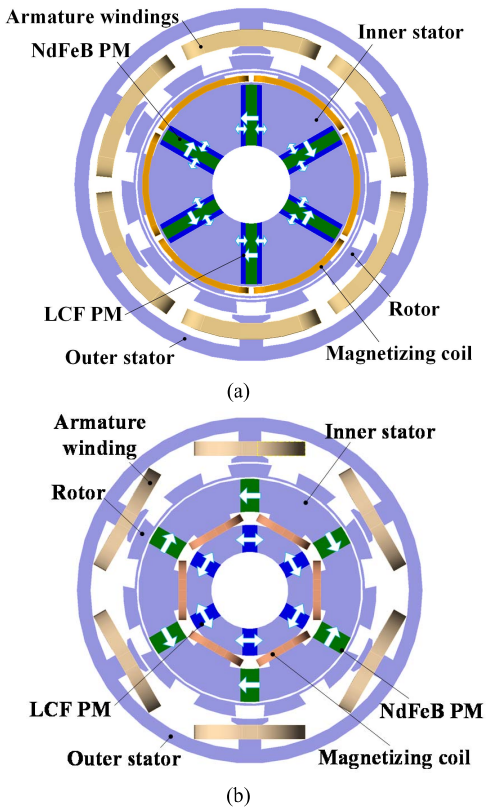

Fig. 1. Topologies of PS-SFMMs. (a) Series type. (b) Parallel type.

the finite-element (FE) method in Section IV. The FE results are validated by the experiments on a parallel prototype in Section V, followed by a conclusion drawn in Section VI.

II. Proposed PS-SFMMs With Parallel and Series Configurations

A. Machine Configurations

The topologies of PS-SFMMs having parallel and series structures are shown in Fig. 1. Both the two machines feature a spoke-type configuration with the same magnet usages. Besides, both the two PS-SFMMs are characterized by the separate PM and armature excitations on the outer and inner stators, respectively. The rotor salient poles are sandwiched between the two stators. The outer stator carrying non-overlapping armature windings is similar to that of the conventional PM machine. The tangentially magnetized LCF PMs behave as flux adjustors, and the NdFeB PMs allow the flux-concentrating effect to increase the torque density. On the other hand, the main difference refers to the magnetic circuit and position of two types of PMs. Evidently, the geometric conflicts between the two sets of windings and hybrid magnets can be alleviated.

B. Flux Regulation Principle

The variable-flux principle of the proposed PS-SFMMs having different magnetic circuit structures can be illustrated by a simplified hysteresis model of LCF PMs, as shown

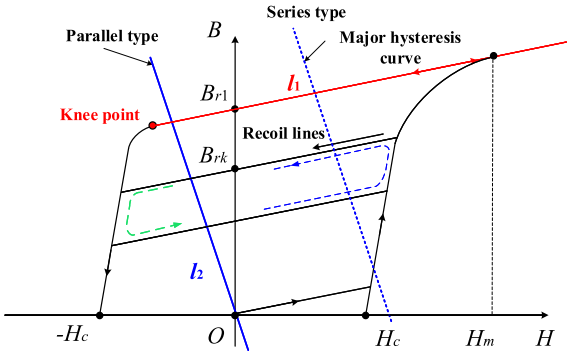

Fig. 2. Flux regulation principle illustrated by the simplified hysteresis model.

in Fig. 2 [10], [13]. First, it can be observed that the coercive force of LCF PM is much lower than that of NdFeB. Thus, the PM working point can be repetitively shifted between different recoil lines by temporarily applying remagnetizing or demagnetizing current pulse. In this model, the major hysteresis loops and all the minor loops are assumed to have identical value of coercive force H_c, but different values of remanence B_{rk}. The set of recoil lines labeled with l_1 can be expressed as

$$B = \mu_0 \mu_r H_m + B_{r1k}, \quad n = 1, 2, 3 \ldots \tag{1}$$

where μ_0 and μ_r are the vacuum permeability and the relative permeability of LCF PM, respectively, H_m is the positive magnetic field intensity, and B_{r1k} represents the corresponding kth remanence of the sets of hysteresis loops.

A magnetization ratio k_{mr} can be defined as the ratio of B_{rk} to the remanence B_{r1}, that is,

$$k_{mr} = B_{rk}/B_{r1}, \quad k = 1, 2, 3 \ldots . \tag{2}$$

Furthermore, from the hysteresis characteristics of two magnetic circuits, the following findings can be summarized.

1) For the series type, the NdFeB magnet will elevate the working point of LCF PMs to a higher level, which is able to stabilize the working point of LCF PM particularly under the on-load operation. However, the required demagnetizing current will be increased in turn. In addition, the flux regulation range is relatively limited due to the strong flux-enhancing effect of NdFeB PMs on LCF PMs.
2) For the parallel case, LCF and NdFeB PMs are located on the two independent branches, and the required magnetizing current and inverter rating will be decreased. Moreover, the flux adjusting range can be designed as sufficiently wide due to the wide variation range of the working point of LCF PMs. Nevertheless, the operating point of LCF PM is quite susceptible to the on-load magnetic field since it is closer to the knee point compared to the series case.

For the two PS-SFMMs, NdFeB PMs serve as a dominant contributor for air-gap flux, while the LCF PMs work as a flux adjustor. Obviously, k_{mr} ranges from -1 to 1, and the air-gap flux can be flexibly adjusted as the magnetization directions of

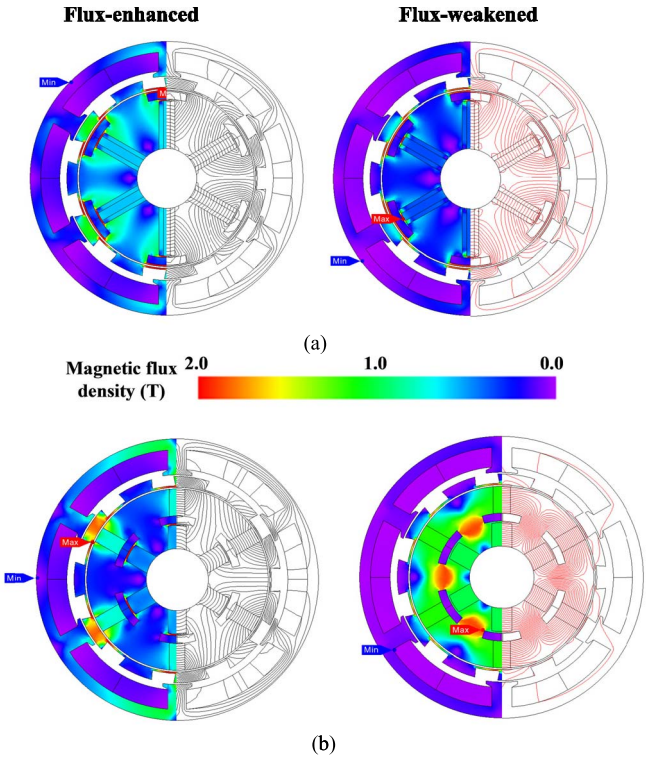

Fig. 3. Simplified illustration of flux lines under different MSs. (a) Series type. (b) Parallel type.

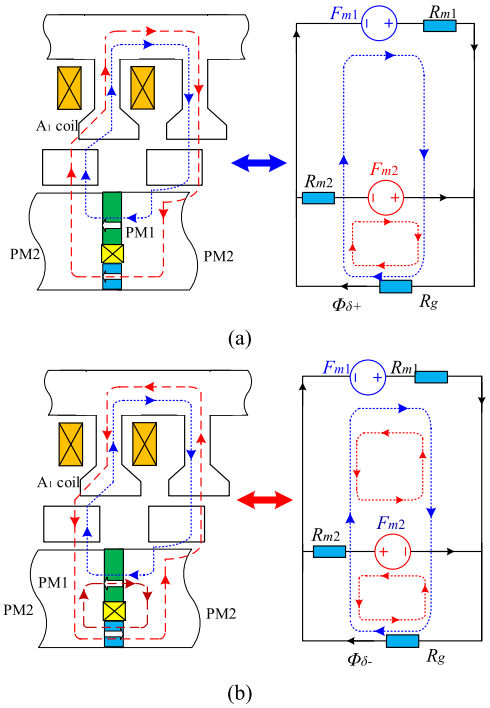

Fig. 4. Simplified magnetic circuit model of the parallel-type PS-SFMM. (a) Flux enhanced. (b) Flux weakened.

LCF magnets are the same or opposite to those of NdFeB PMs, i.e., so-called the flux-enhanced and flux-weakened states, as represented by the open-circuit field distributions shown in Fig. 3. Therefore, for low-speed region, NdFeB and LCF PMs are with the same magnetization directions, the torque density can be subsequently improved. On the other hand, for high-speed region, LCF PMs are reversely demagnetized to weaken the NdFeB PM fields, and hence the effective FW can be achieved to effectively extend CPSR within the limitation of the inverter power rating.

III. Analytical Modeling for PM Sizing Optimization

The optimal magnet hybrid ratio is recognized as a key issue for PS-SFMM design. Instead of the time-consuming FE analysis, a simplified magnetic circuit method is developed to facilitate the optimization approach of the PM sizing. Consequently, in order to analytically reveal the underlying design tradeoff, both the parallel and series magnetic circuits are investigated here.

A. Simplified Magnetic Circuits

The simplified magnetic circuits of the spoke-type PS-SFMMs with series and parallel PM arrangements are portrayed in Figs. 4 and 5, which neglect the magnetic reluctances of iron parts. First, for the parallel case, the air-gap fluxes $\Phi_{\delta+}$ and $\Phi_{\delta-}$ at the flux-enhanced and flux-weakened states can be analytically formulated for the further optimization [15]

$$\Phi_{\delta+} = \frac{H_{c2}\mu_0\mu_{r2}A_{m2} + H_{c1}\mu_0\mu_{r1}A_{m1}}{R_g\left(\frac{\mu_0\mu_{r1}}{h_{m1}}A_{m1} + \frac{\mu_0\mu_{r2}}{h_{m2}}A_{m2}\right) + 1} \tag{3}$$

$$\Phi_{\delta-} = \frac{H_{c2}\mu_0\mu_{r2}A_{m2} - H_{c1}\mu_0\mu_{r1}A_{m1}}{R_g\left(\frac{\mu_0\mu_{r1}}{h_{m1}}A_{m1} + \frac{\mu_0\mu_{r2}}{h_{m2}}A_{m2}\right) + 1} \tag{4}$$

where H_{c1} and H_{c2} are the coercive forces of LCF and NdFeB PMs, respectively, h_{m1} and h_{m2} are the thicknesses of LCF and NdFeB PMs, respectively, A_{m1} and A_{m2} are the cross-sectional areas of LCF and NdFeB PMs, respectively, μ_{r1} and μ_{r2} are the relative permeabilities of LCF and NdFeB PMs, respectively, μ_o is the vacuum permeability, and R_g is the air-gap magnetic reluctance.

The flux adjusting ratio α_{mag} is defined as the ratio of $\Phi_{\delta+}$ to $\Phi_{\delta-}$ for characterizing the air-gap flux control range, that is,

$$\alpha_{\text{mag}} = \frac{H_{c2}\mu_{r2}A_{m2} + H_{c1}\mu_{r1}A_{m1}}{H_{c2}\mu_{r2}A_{m2} - H_{c1}\mu_{r1}A_{m1}} = \frac{\frac{H_{c2}\mu_{r2}A_{m2}}{H_{c1}\mu_{r1}A_{m1}} + 1}{\frac{H_{c2}\mu_{r2}A_{m2}}{H_{c1}\mu_{r1}A_{m1}} - 1}. \tag{5}$$

As for the series type, the corresponding open-circuit air-gap fluxes $\Phi'_{\delta+}$ and $\Phi'_{\delta-}$ at the flux-enhanced and flux-weakened states can be analogously represented as

$$\Phi'_{\delta+} = \frac{H_{c1}h_{m1} + 2H_{c2}h_{m2}}{(R_{g1} + R_{g2}) + \frac{h_{m1}}{\mu_0\mu_{r1}A_{m1}} + \frac{2h_{m2}}{\mu_0\mu_{r2}A_{m2}}} \tag{6}$$

$$\Phi'_{\delta-} = \frac{H_{c1}h_{m1} - 2H_{c2}h_{m2}}{(R_{g1} + R_{g2}) + \frac{h_{m1}}{\mu_0\mu_{r1}A_{m1}} + \frac{2h_{m2}}{\mu_0\mu_{r2}A_{m2}}} \tag{7}$$

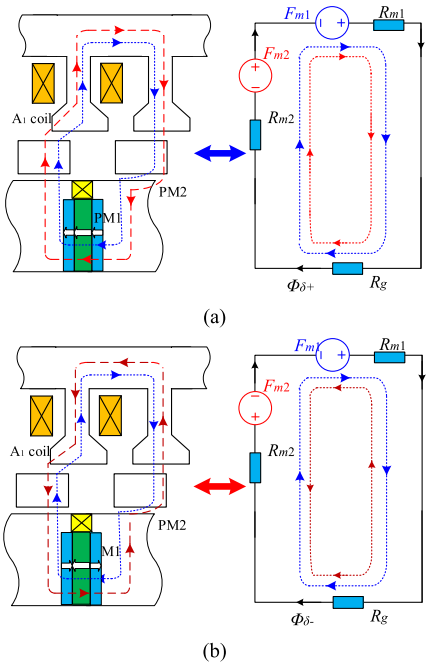

Fig. 5. Simplified magnetic circuit model of the series-type PS-SFMM. (a) Flux enhanced. (b) Flux weakened.

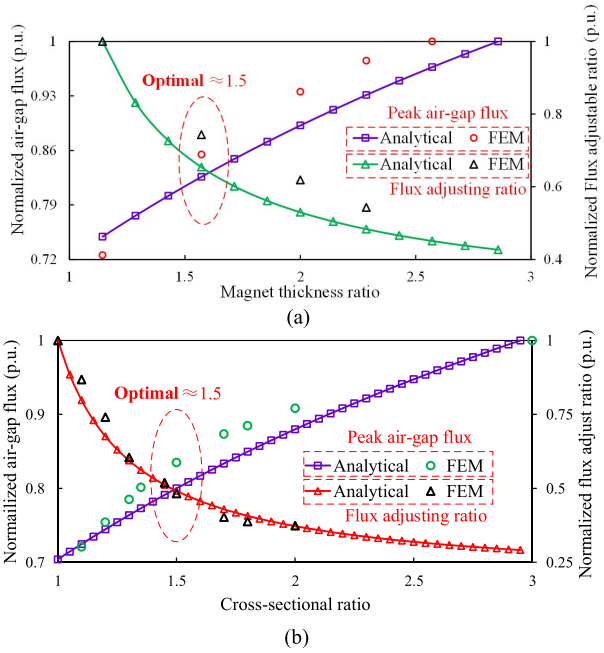

Fig. 6. Comparison of FE and analytically predicted normalized torque capability and flux adjusting ratio. (a) Series type. (b) Parallel type.

and the flux adjusting ratio α'_{mag} can be expressed as

$$\alpha'_{\text{mag}} = \frac{H_{c1}h_{m1} + 2H_{c2}h_{m2}}{H_{c1}h_{m1} + 2H_{c2}h_{m2}} = \frac{\frac{H_{c1}h_{m1}}{H_{c2}h_{m2}} + 2}{\frac{H_{c1}h_{m1}}{H_{c2}h_{m2}} - 2}. \tag{8}$$

B. Design Tradeoffs

With the aid of the magnetic circuit model, the magnet sizing should be optimized as a key parameter. The variations of the normalized maximum air-gap flux and flux adjusting ratio with the magnet cross-sectional ratio (A_{m2}/A_{m1}) of DS-SFMM are calculated and compared with the FE results shown in Fig. 6. It shows that there is a design tradeoff between the torque capability and flux regulation range in both two PS-SFMMs [15]. In addition, it can be observed that the key performance is mainly determined by the magnet cross-sectional and thickness ratios for the parallel and series cases, respectively. Meanwhile, the optimal magnet cross-sectional and thickness ratios for the parallel and series cases can be obtained, i.e., ∼1.5, which well balances the torque capability and flux adjusting range. As a result, the design parameters can be optimized based on the constraints of optimal magnet sizing ratio, fixed copper loss of 30 W, and zero d-axis current control under the flux-enhanced state. The optimized design parameters are tabulated in Table I. For the sake of fair comparison, the two machines are designed with the same overall dimensions, PM usages, and rated current. It should be noted that the fully demagnetizing current of the series-type PS-SFMM is 2.4 times that of its parallel counterpart, which is mainly attributed to the large magnetic reluctance of two-layer PMs, as well as the stabilizing effect of the NdFeB magnets on the working point of LCF PMs, as mentioned earlier.

TABLE I
KEY DESIGN PARAMETERS OF THE PS-SFMMS WITH SERIES AND PARALLEL STRUCTURES

Machine types	Series	Parallel
Rated speed (r/min)	400	
Rated current (Arms)	17.5	
Outer diameter of outer stator (mm)	90	
Inner diameter of outer stator (mm)	56	
Outer stator tooth arc (deg.)	13	12
Outer stator tooth-tip width (mm)	6.5	
Outer diameter of inner stator (mm)	56	
Outer air-gap length (mm)	0.5	
Inner air-gap length (mm)	0.5	
Arc of outer/inner rotor (deg.)	14/16	18/19
Rotor segment thickness (mm)	5	
Active stack length (mm)	25	
LCF PM thickness×length (mm)	2.4/10	4.0/6
NdFeB PM thickness×length (mm)	1.6/10	3.2/5
PM volume (cm^3)	116.10	
NdFeB PM grade	N35SH	
NdFeB PM remanence	1.2T	
LCF PM grade	SB12B	
LCF PM remanence	0.8T	
Number of armature turns per coil	84	
Number of magnetizing turns per coil	100	
Steel grade	35CS440	
Fully demagnetizing current (A)	44.6	18.5

IV. ELECTROMAGNETIC PERFORMANCE COMPARISON

A. Flux Regulation Performance

The open-circuit back EMFs of the two PS-SFMMs under different MSs are plotted in Fig. 7. Obviously, the parallel-type machine exhibits the higher EMF magnitude at the flux-enhanced state. Moreover, the variation of the fundamental back EMFs at 400 r/min with the magnetization ratio of LCF PMs is shown in Fig. 8. It can be seen that the parallel-type PS-SFMM exhibits significantly wider flux regulation range due to the enhancing effect of NdFeB field on the working point of LCF PMs.

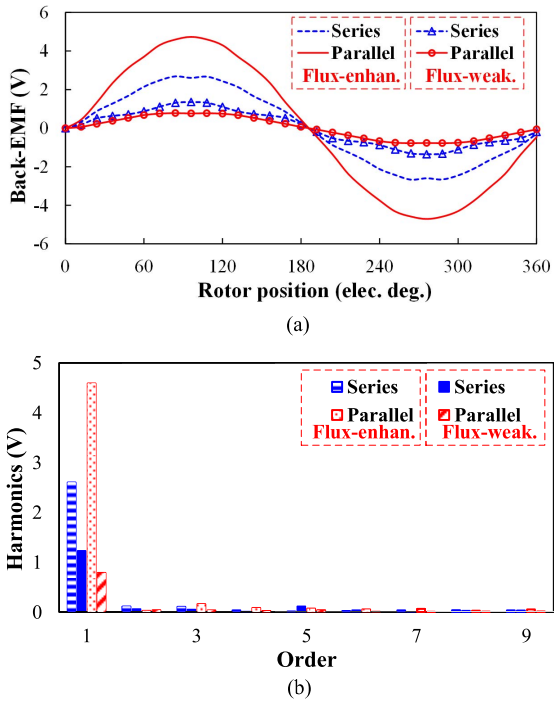

Fig. 7. Open-circuit back EMFs under different MSs. (a) Waveforms. (b) Harmonic spectra, 400 r/min.

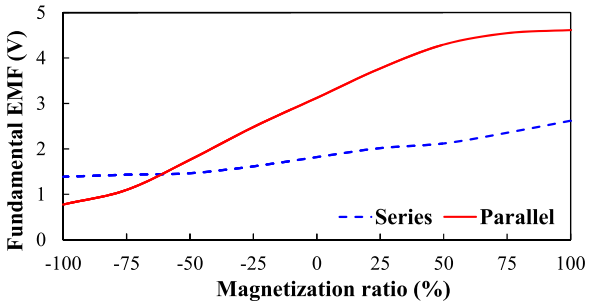

Fig. 8. Variation of back-EMF fundamental magnitudes with the magnetization ratio, 400 r/min.

B. Torque Performance

Fig. 9(a) shows the cogging torques under the flux-enhanced state. The parallel-type PS-SFMM shows slightly higher than its series counterpart. The torque against current angle characteristic is investigated in Fig. 9(b) in advance so as to seek the maximum torque per ampere control strategy. It shows that the unity saliency ratio can be observed in the two PS-SFMMs. In addition, the torque characteristics of the machines under zero d-axis current control are investigated. The steady-state torque waveforms under rated current are shown in Fig. 9(c). It can be observed that the parallel machine exhibits higher torque capability, together with the slightly higher torque ripple that is consistent with the cogging torque results illustrated in Fig. 9(a). Fig. 9(d) shows the torque versus current curves. It demonstrates that the parallel machine exhibits higher torque regardless of loads.

C. Armature Demagnetization Withstand Capability

The armature reaction fields in the two machines at rated load are shown in Fig. 10 by the frozen permeability

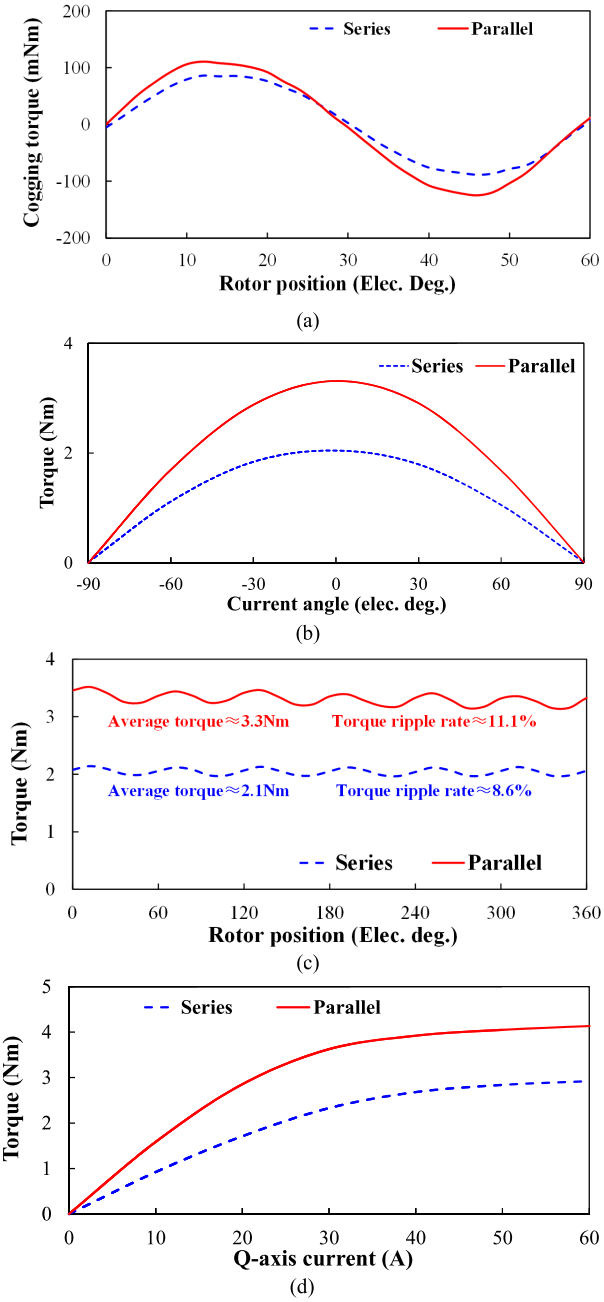

Fig. 9. Torque characteristics of PS-SFMMs with series and parallel configurations under the flux-enhanced state. (a) Cogging torque. (b) Torque–current angle characteristics, phase current = 17.5 Arms. (c) Steady-state torque waveforms, phase current = 17.5 Arms. (d) Torque against current curves.

method [18]. Obviously, there are little armature fields penetrating LCF PMs in both two machines. Besides, the on-load demagnetization behavior of LCF PMs is investigated. The variation of working point of the LCF PM before and after applying a q-axis current of 50 A is shown in Fig. 11. It demonstrates that better demagnetization withstand capability can be observed in the series case, which is mainly due to the stabilizing effect of the NdFeB PM field.

D. Iron Loss

The iron loss characteristics of the two PS-SFMMs are evaluated as shown in Fig. 12. It shows that the parallel-type

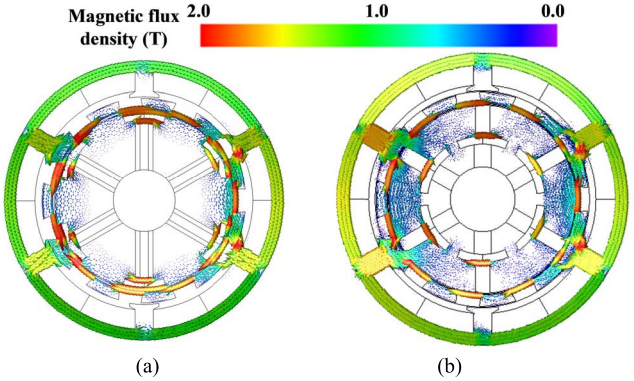

Fig. 10. Armature fields under the rated load. (a) Series type. (b) Parallel type.

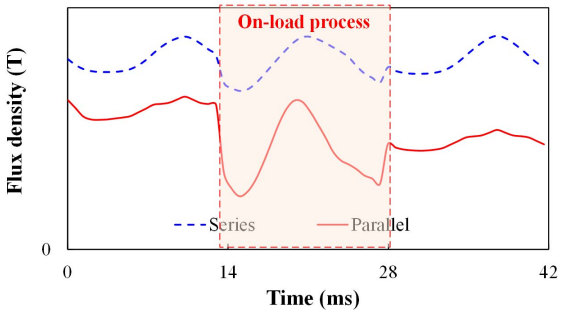

Fig. 11. Working point variation of the LCF PM subject to a q-axis current pulse, 2* rated load.

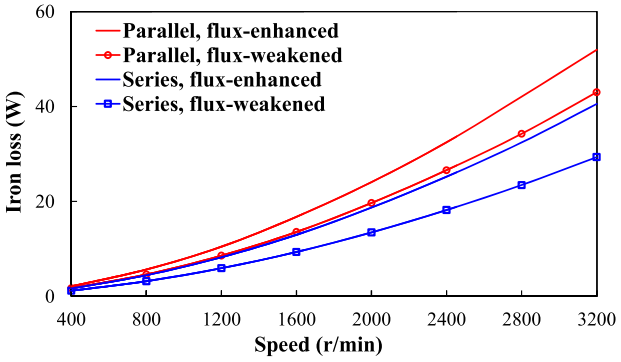

Fig. 12. Rated-load iron loss characteristics of the proposed PS-SFMMs under different MSs.

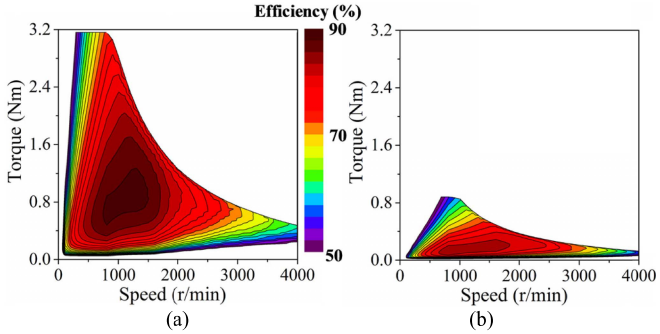

Fig. 13. Efficiency maps of the parallel-type PS-SFMM under different MSs. (a) Flux enhanced. (b) Flux weakened. (DC link voltage = 36 V and rated rms current = 17.5 A.)

exhibits lower iron losses than the series counterpart regardless of MS, which is mainly attributed to less magnetic saturation in the series-type case. In addition, the iron loss can be further

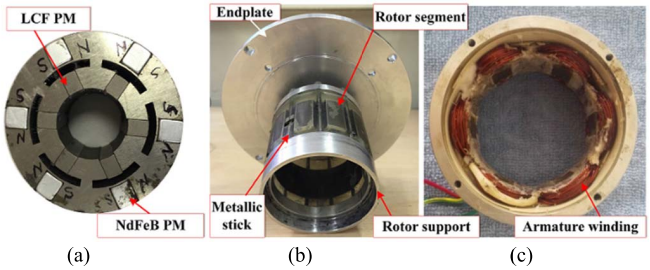

Fig. 14. Parallel-type PS-SFMM prototype. (a) Inner stator. (b) Rotor. (c) Outer stator.

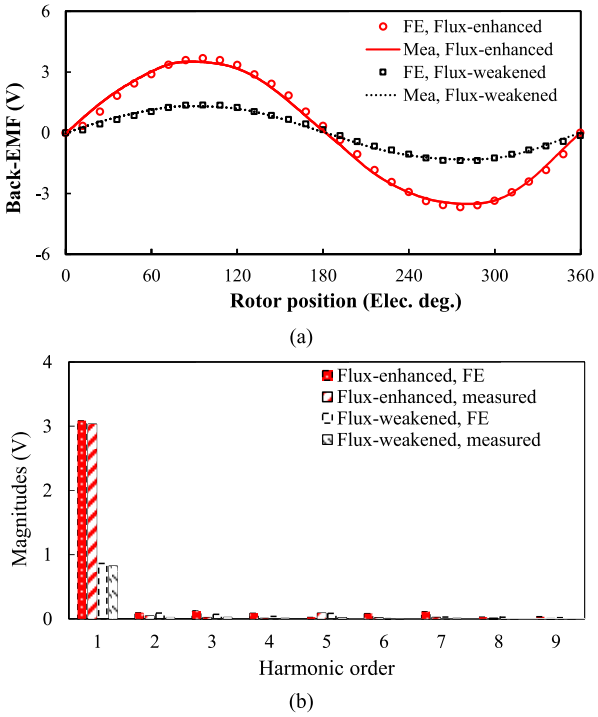

Fig. 15. Comparison of predicted and measured back-EMF waveforms under different MSs, 400 r/min. (a) Waveform. (b) Harmonic spectra.

reduced by demagnetizing LCF PMs, which is beneficial for the efficiency improvement over high-speed operation.

E. Efficiency Maps

Due to the satisfactory torque quality and wide MS control range, the parallel-type PS-SFMM is selected for the following efficiency investigation [19]. The efficiency maps under different MSs are plotted in Fig. 13. The results confirm that the proposed PS-SFMM can achieve high efficiency within a wide range of speeds and loads by combing the highest efficiency characteristics corresponding to appropriate MS under different operating regions.

V. Experimental Validation

In order to validate the previous FE analyses, a 6-/11-pole PSMM prototype with parallel configuration is manufactured and tested to verify the feasibility of the proposed design. The stator and rotor assemblies are shown in Fig. 14. The FE-predicted and measured open-circuit

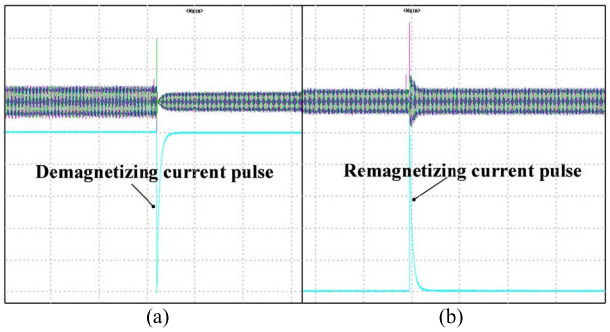

Fig. 16. Responses of open-circuit phase back EMF (400 r/min) to a current pulse and EMF (5 V/div), Current (10 A/div), and time (200 ms/div). (a) Demagnetization. (b) Remagnetization.

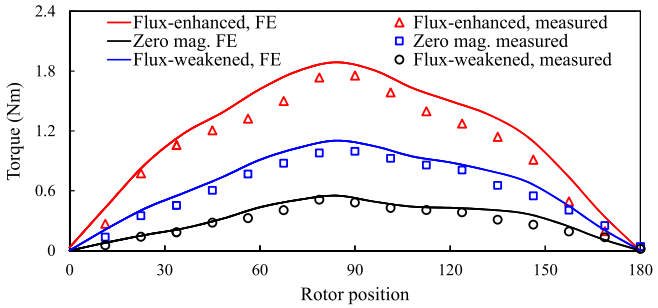

Fig. 17. Comparison of predicted and measured static torques against rotor position, $I_a = -2 \times I_b = -2 \times I_c = 17.5$ A.

phase back EMFs at various MSs are compared with the FE predictions shown in Fig. 15. Moreover, the transient responses of the open-circuit phase back EMFs for remagnetizing and demagnetizing current pulses are shown in Fig. 16, which confirms the excellent flux control capability of the proposed machine. The FE-predicted and tested static torques versus rotor position characteristics are shown in Fig. 17. It can be seen that the parallel-type PS-SFMM machine shows excellent flux regulation capability, which agrees well with the preceding analyses. Overall, a good agreement can be obtained between the measured and FE-predicted results.

VI. Conclusion

In this paper, a comparative study of novel PS-SFMMs having parallel and series hybrid magnet arrangements are presented. Due to the alleviation of geometric conflicts between PM excitation and armature winding, the proposed machines take the advantages of improved torque density compared to the single-stator counterparts. Based on the simplified magnetic circuit models, the design tradeoffs and design considerations for the PM sizing are analytically revealed and investigated. It shows that the optimal PM cross-sectional and thickness ratios for the parallel as well as series cases are approximately 1.5, which can well balance the torque capability and flux regulation range. The electromagnetic characteristics of the two PS-SFMMs are comprehensively compared. It can be found that a better armature demagnetization withstand capability and lower torque ripple can be observed in the series type, whereas the parallel machine exhibits lower fully demagnetizing current, higher torque capability, and wider flux regulation range, as well as high efficiency over a wide operating range, which is desirable for wide-speed-range applications.

Acknowledgment

This work was jointly supported in part by National Natural Science Foundations of China under Grant 51377036, in part by Natural Science Foundation of Jiangsu Province for Youth (BK20170674), in part by the Fundamental Research Funds for the Central Universities (2242017K41003), in part by âŁœHong Kong ScholarâŁž Program (XJ2018014), in part by Supported by the "excellent young scholars" Program of Southeast University, and in part the Scientific Research Foundation of Graduate School of Southeast University.

References

[1] K. T. Chau, C. C. Chan, and C. Liu, "Overview of permanent-magnet brushless drives for electric and hybrid electric vehicles," *IEEE Trans. Ind. Electron.*, vol. 55, no. 6, pp. 2246–2257, Jun. 2008.

[2] W. L. Soong and T. J. E. Miller, "Field-weakening performance of brushless synchronous AC motor drives," *IEE Proc.-Electr. Power Appl.*, vol. 141, no. 6, pp. 331–340, Nov. 1994.

[3] H. Yang, Z. Q. Zhu, H. Lin, and W. Q. Chu, "Flux adjustable permanent magnet machines: A technology status review," *Chin. J. Elect. Eng.*, vol. 2, no. 2, pp. 14–30, Dec. 2016.

[4] V. Ostovic, "Memory motors," *IEEE Ind. Appl. Mag.*, vol. 9, no. 1, pp. 52–61, Jan./Feb. 2003.

[5] K. Sakai, K. Hagiwara, and Y. Hirano, "High-power and high-efficiency permanent-magnet reluctance motor for hybrid electric vehicle," *TOSHIBA Rev. Jpn.*, vol. 60, no. 11, pp. 41–44, Sep. 2005.

[6] S. Maekawa *et al.*, "Study of the magnetization method suitable for fractional-slot concentrated-winding variable magnetomotive-force memory motor," *IEEE Trans. Power Electron.*, vol. 29, no. 9, pp. 4877–4887, Sep. 2014.

[7] A. Athavale, K. Sasaki, B. S. Gagas, T. Kato, and R. D. Lorenz, "Variable flux permanent magnet synchronous machine (VF-PMSM) design methodologies to meet electric vehicle traction requirements with reduced losses," *IEEE Trans. Ind. Appl.*, vol. 53, no. 5, pp. 4318–4326, Sep./Oct. 2017.

[8] M. Ibrahim, L. Masisi, and P. Pillay, "Design of variable flux permanent-magnet machine for reduced inverter rating," *IEEE Trans. Ind. Appl.*, vol. 51, no. 5, pp. 3666–3674, Sep./Oct. 2015.

[9] C. Yu and K. T. Chau, "Design, analysis, and control of DC-excited memory motors," *IEEE Trans. Energy Convers.*, vol. 26, no. 2, pp. 479–489, Jun. 2011.

[10] Y. Gong, K. T. Chau, J. Z. Jiang, C. Yu, and W. Li, "Analysis of doubly salient memory motors using Preisach theory," *IEEE Trans. Magn.*, vol. 45, no. 10, pp. 4676–4679, Oct. 2009.

[11] X. Zhu, L. Quan, D. Chen, M. Cheng, W. Hua, and X. Sun, "Electromagnetic performance analysis of a new stator-permanent-magnet doubly salient flux memory motor using a piecewise-linear hysteresis model," *IEEE Trans. Magn.*, vol. 47, no. 5, pp. 1106–1109, May 2011.

[12] X. Zhu, L. Quan, D. Chen, M. Cheng, Z. Wang, and W. Li, "Design and analysis of a new flux memory doubly salient motor capable of online flux control," *IEEE Trans. Magn.*, vol. 47, no. 10, pp. 3220–3223, Oct. 2011.

[13] H. Yang, H. Lin, J. Dong, J. Yan, Y. Huang, and S. Fang, "Analysis of a novel switched-flux memory motor employing a time-divisional magnetization strategy," *IEEE Trans. Magn.*, vol. 50, no. 2, pp. 849–852, Feb. 2014.

[14] D. Wu, X. Liu, Z. Q. Zhu, A. Pride, R. Deodhar, and T. Sasaki, "Switched flux hybrid magnet memory machine," *IET Electr. Power Appl.*, vol. 9, no. 11, pp. 160–170, Feb. 2015.

[15] H. Yang, Z. Q. Zhu, H. Lin, and S. Lyu, "Comparative study of hybrid PM memory machines having single- and dual-stator configurations," *IEEE Trans. Ind. Electron.*, vol. 65, no. 11, pp. 9168–9178, Nov. 2018.

[16] H. Yang, Z.-Q. Zhu, H. Lin, S. Fang, and Y. Huang, "Synthesis of hybrid magnet memory machines having separate stators for traction applications," *IEEE Trans. Veh. Technol.*, vol. 67, no. 1, pp. 183–195, Jan. 2018.

[17] H. Yang *et al.*, "Analysis of on-load magnetization characteristics in a novel partitioned stator hybrid magnet memory machine," *IEEE Trans. Magn.*, vol. 53, no. 6, Jan. 2017, Art. no. 8103404.
[18] W. Q. Chu and Z. Q. Zhu, "Average torque separation in permanent magnet synchronous machines using frozen permeability," *IEEE Trans. Magn.*, vol. 49, no. 3, pp. 1202–1210, Mar. 2013.
[19] W. Q. Chu, Z. Q. Zhu, J. Zhang, X. Liu, D. A. Stone, and M. P. Foster, "Investigation on operational envelops and efficiency maps of electrically excited machines for electrical vehicle applications," *IEEE Trans. Magn.*, vol. 51, no. 4, Apr. 2015, Art. no. 8103510,

Hui Yang (S'13–M'16) was born in Changning, Hunan, China. He received the B.Eng. degree in electrical engineering from the Dalian University of Technology, Dalian, China, in 2011, and the Ph.D. degree in electrical engineering from Southeast University, Nanjing, China, in 2016.

From 2014 to 2015, he was supported by the China Scholarship Council through a one-year joint Ph.D. studentship at The University of Sheffield, Sheffield, U.K. Since 2016, he has been with Southeast University, where he has been a Lecturer with the School of Electrical Engineering. He holds 11 patents. His current research interests include design and analysis of novel permanent-magnet machines with particular reference to variable-flux machines for electric vehicles and renewable energy applications.

Dr. Yang was a recipient of the Best Paper Award in ICEMS 2014 and Best Paper Award in EVER 2015.

Hao Zheng received the B.Eng. degree in electrical engineering from Nanjing Normal University, Nanjing, China, in 2017. He is currently pursuing the M.Eng. degree in electrical engineering with Southeast University, Nanjing, China.

His current research interests include design and analysis of permanent-magnet machines especially memory machine.

Z. Q. Zhu (M'90–SM'00–F'09) received the B.Eng. and M.Sc. degrees in electrical and electronic engineering from Zhejiang University, Hangzhou, China, in 1982 and 1984, respectively, and the Ph.D. degree in electrical and electronic engineering from The University of Sheffield, Sheffield, U.K., in 1991.

Since 1988, he has been with The University of Sheffield, where he is currently a Professor with the Department of Electronic and Electrical Engineering, the Head of the Electrical Machines and Drives Research Group, the Royal Academy of Engineering/Siemens Research Chair, the Academic Director of the Sheffield Siemens Wind Power Research Centre, the Director of the Sheffield CRRC Electric Drives Technology Research Centre. His current research interests include the design and control of permanent-magnet brushless machines and drives for applications ranging from automotive to renewable energy.

Dr. Zhu is a fellow of the Royal Academy of Engineering, U.K.

Heyun Lin (M'13–SM'13) received the B.S., M.S., and Ph.D. degrees in electrical engineering from the Nanjing University of Aeronautics and Astronautics, Nanjing, China, in 1985, 1989, and 1992, respectively.

From 1992 to 1994, he was a Post-Doctoral Fellow with Southeast University, Nanjing. In 1994, he joined the School of Electrical Engineering, Southeast University, as an Associate Professor and became a Full Professor since 2000. He has authored over 150 technical papers and holds 30 patents. His current research interests include the design, analysis and control of permanent magnet motor, intelligent electrical apparatus, and electromagnetic field numerical analysis.

Dr. Lin is a fellow of IET, a member of the Electrical Motor and Apparatus Committee of Jiangsu Province, and a Senior Member of the China Society of Electrical Engineering and the China Electrotechnical Society.

Shukang Lyu received the B.Eng. degree in new energy science and engineering from Hohai University, Nanjing, China, in 2016. He is currently pursuing the Ph.D. degree in electrical engineering with Southeast University, Nanjing, China.

His current research interests include control strategies for permanent magnet machines and power electronics.

Zhenbao Pan was born in Guilin, China. He received the B.S. degree in electrical engineering and automation and the M.S. degree in detection technology and automatic equipment from Anhui University, Hefei, China, in 2014 and 2017, respectively. He is currently pursuing the Ph.D. degree in electrical engineering with the School of Electrical Engineering, Southeast University, Nanjing, China.

His current research interests include the design, analysis, and optimization and control of electrical machines.